Bulletin of the Seismological Society of America, Vol. 97, No. 3, pp. 901–914, June 2007, doi: 10.1785/0120060066

Assessment of a Nonlinear Dynamic Rupture Inversion Technique Applied to a Synthetic Earthquake

by Siobhan M. Corish, Chris R. Bradley, and Kim B. Olsen

Abstract Dynamic rupture inversion is a powerful tool for learning why and how faults fail, but much more work has been done in developing inversion methods than evaluating how well these methods work. This study examines how well a nonlinear rupture inversion method recovers a set of known dynamic rupture parameters on a synthetic fault based on the 2000 western Tottori, Japan earthquake (M_w 6.6). Rupture evolution on the fault is governed by a slip-weakening friction law. A direct-search method known as the neighborhood algorithm (Sambridge, 1999) is used to find optimal values of both the initial stress distribution and the slip-weakening distance on the fault, based on misfit values between known and predicted strong-motion displacement records. The yield stress and frictional sliding stress on the fault are held constant. A statistical assessment of the results shows that, for this test case, the inversion succeeds in locating all parameters to within $\pm 14\%$ of their true values. With the model configuration used in this study, the parameters located in the central rupture area are better resolved than the parameters located at the sides and bottom of the fault. In addition, a positive linear correlation between the mean initial stress and the slip-weakening distance is identified. The investigation confirms that dynamic rupture inversion is useful for determining rupture parameters on the fault, but that intrinsic trade-offs and poor resolution of some parameters limit the amount of information that can be unambiguously inferred from the results. In addition, this study demonstrates that using a statistical approach to assess nonlinear inversion results shows how sensitive the misfit measure is to the various parameters, and allows a level of confidence to be attached to the output parameter values.

Introduction

Catastrophic rupture of large earthquakes occurs when conditions on a fault plane achieve a critical configuration. Finding out precisely what conditions existed on a fault at the time of rupture is a vital part of learning why and how faults fail and predicting where future earthquakes might strike. Because rupture parameters within the earth are difficult to measure in the field or replicate in the laboratory, numerical inversion of the rupture problem using near-fault strong-motion data is one of the strongest tools available for determining the details of a rupture and the conditions that caused it. Increasingly, dynamic models of spontaneous rupture propagation (e.g., Madariaga *et al.*, 1998; Peyrat and Olsen, 2004) are used to analyze strong-motion data. Unlike kinematic models (e.g., Cotton and Campillo, 1995; Zhang *et al.*, 2003), which prescribe a slip function that determines ground motions, a dynamic approach explicitly solves the mechanical problem of rupture, subject to plausible stress constraints, and can provide useful insights about how faults rupture.

In a dynamic fault rupture model, the stresses acting on the fault are specified, along with a set of constitutive equations describing how the material around the fault translates stresses into motion. In the case of spontaneous dynamic rupture propagation, rupture on the fault is completely determined by the stresses acting on the fault and the constitutive equations. The final slip, slip pattern, rupture velocity, and the radiated waves all emerge as solutions from the rupture problem.

To model dynamic rupture, physically plausible constitutive relations must be defined for the fault zone. A slip-weakening friction law (Ida, 1972; Andrews, 1976; Day, 1982) is commonly used. According to this law, frictional resistance to slip holds the fault locked until the shear stress reaches a critical level, known as the yield stress. Once slip begins, the shear stress decreases linearly, over a finite length called the slip-weakening distance, to a dynamic frictional sliding level. The slip-weakening distance is introduced to maintain finite levels of stress and slip rate at the rupture front. Earthquakes are sensitive only to changes in the stress state on a fault rather than to the absolute level of stress, so

the frictional sliding stress is often set to 0, and all other stresses are defined relative to this mark. The slip-weakening relation is then completely parameterized by the yield stress (T_u) and the slip-weakening distance (D_c). T_u, D_c, and the initial stress (T_e), are the dynamic rupture parameters used in this study. Together, these parameters shape the rupture pattern on the fault and the resulting radiated waves.

Spontaneous dynamic rupture is a strongly nonlinear problem for which no simple analytical solution exists, so determining the dynamic rupture parameters from seismic data requires a nonlinear, numerical inverse procedure. The inverse procedure typically works as follows. Initial guesses of the rupture parameters are incorporated into a forward model that propagates rupture according to a three-dimensional elastic wave equation, and the resulting ground motions are compared with observations. Parameter values are refined by an iterative process in which the parameter space is sampled by an efficient direct-search algorithm, and each set of values found is plugged into the forward model until a good match to the observed seismic waveforms is achieved. A direct-search algorithm is employed instead of a gradient method because the relationship between the dynamic rupture parameters and the strong-motion records can be extremely nonlinear. The use of nonlinear dynamic inversion methods to infer fault characteristics from strong-motion data has been shown to yield promising results (Peyrat and Olsen, 2004), but so far, no systematic appraisal of the inversion process has been done to determine its specific capabilities and limitations. Like other geophysical inverse problems, the solutions to strong-motion dynamic inversions are not necessarily unique, and furthermore, all parameters cannot be determined equally well. To make meaningful inferences about the state of a fault from dynamic inversion results, it is extremely important to be aware of the possible ambiguities in the results and to acknowledge when parameters might not be well constrained by the inversion.

This study tests how well a nonlinear inversion method reproduces a known set of dynamic rupture parameters from synthetic strong-motion displacement records. The parameters used to generate the known ground-motion response are based on inversion solutions of data from the 2000 western Tottori, Japan earthquake (M_w 6.6) (Peyrat and Olsen, 2004; S. M. Corish, C. R. Bradley, and K. B. Olsen, unpublished data, 2005). There are two reasons for using a synthetic set of dynamic rupture parameters for this test. First, the parameters are known exactly and therefore provide an explicit point of comparison for the inversion results, and second, the inversion parameters can be defined in precisely the same terms as the true parameters, thereby isolating the inversion problem itself from errors due to unknowns in the real earth. Comparison of the inversion results with the true parameters offers a quantitative determination of the ability of the inversion process to resolve the known parameters. Further, a statistical analysis of the results demonstrates how well each parameter can be constrained by the inversion, and gauges ambiguity, in the form of trade-off between parameters. The findings from this study can be applied to more complex inversions using real data.

Method

The inversion is carried out using a direct-search method known as the neighborhood algorithm (Sambridge, 1999), which concentrates the parameter search in nearest-neighbor regions about the current best-fitting parameter sets. This algorithm has been used previously to invert strong-motion data for a heterogeneous initial stress distribution on a fault (Peyrat and Olsen, 2004). In the current investigation, the neighborhood algorithm is used to find optimal values of both initial stress and slip-weakening distance parameters on a fault, based on least-squares misfit values between the known and computed seismograms.

Sambridge's neighborhood algorithm works as follows: (1) an initial group of n_{so} sets of parameters is generated randomly, using uniform random sampling in the multi-dimensional parameter space (see Table 2 for parameter ranges). (2) The forward dynamic rupture simulation is run for each generated set of parameters, and misfit values are calculated, based on a comparison between the computed and "true" seismograms. (3) The entire parameter space is divided into nearest-neighbor regions about each set. Each nearest-neighbor region consists of all points in the space that are closer to a particular set than to any other, as defined by an L_2 norm. (4) The misfits of all the parameter sets are ranked, and n_s new parameter sets are generated in the nearest-neighbor regions about the n_r sets with the lowest misfit values. The process is repeated until an acceptable convergence is reached.

The neighborhood algorithm has several advantages over other direct-search methods. First, exploitation of the nearest-neighbor construct quickly guides the search to good-fitting areas of the parameter space: in each iteration, sampling is concentrated in the regions of the parameter space that have produced better fits to the true seismograms. Second, only two control variables are required to configure the search: n_s, the number of new sets of parameters generated per iteration, and n_r, the number of nearest-neighbor cells resampled in each generation. In the current investigation, $n_s = 40$ and $n_r = 14$ were found, after some experimentation, to provide a good balance between the speed of convergence and the exhaustiveness of the search.

Spontaneous propagation of a dynamic rupture constitutes the forward problem. Rupture occurs on a vertical, planar fault within a three-dimensional medium. The forward problem is solved by applying a fourth-order, staggered-grid finite-difference scheme to a velocity-stress formulation of the three-dimensional elastic wave equation (Olsen, 1994; Graves, 1996). The finite-difference implementation largely follows Madariaga *et al.* (1998), but the fault-plane boundary condition has been updated to a more accurate stress-glut formulation (Andrews, 1999).

The earth model, containing the fault and nine nearby strong-motion stations, is 40 km parallel to the fault strike, by 40 km perpendicular to strike, by 16 km deep. The fault itself strikes 150°, and extends 24 km along strike and 15 km down dip (vertical). Rupture proceeds in a left-lateral sense. The top of the fault is 1 km below the surface, and the hypocenter is located at a depth of 11 km. The grid spacing used in the model is $dx = 500$ m (Fig. 1). Current computational resources prevent using much smaller grid spacing for the forward simulation because, for the finite-difference scheme used here, computational cost increases with the fourth power of the grid spacing. Thus, decreasing the grid spacing to 100 m increases the computation time by a factor of 625. However, it will be demonstrated that the 500-m grid produces results that are comparable to those produced by a 100-m grid.

The velocity structure used for the Tottori region is shown in Table 1. The stability criterion for the finite-difference approximation requires that $v_{\max} \times dt/dx < 0.5$, where $v_{\max}$ is the maximum *P*-wave velocity encountered in the medium (Moczo *et al.*, 2000). From Table 1, $v_{\max}$ is 6.5 km/sec, and $dx = 500$ m, so $dt = 0.025$ sec satisfies the criterion. The finite-difference calculations are carried out every 0.025 sec for a total of 20 sec.

A free-surface boundary condition (FS2 of Gottschaemmer and Olsen, 2001) is included along the top surface of the earth model, and an efficient, perfectly matched layers (PML) absorbing boundary condition (Marcinkovich and Olsen, 2003) is imposed along the remaining grid boundaries to minimize unphysical wave reflections from the sides of the model. A stress-glut condition, which computes the slip and the slip rate on the fault from the fault-plane strain (Andrews, 1999), is imposed at the fault-plane boundary.

Rupture is initiated artificially by lowering the yield stress to zero in a 2.5-km-square patch at the hypocentral location. A 3-sec time window is allowed for a particular parameter set to induce rupture; if a rupture does not initiate within this time, the parameter set is assigned a high misfit value and the inversion moves to the next set. After initiation, further evolution of the rupture is controlled entirely by the dynamic rupture parameters: the initial stress (T_e), the slip-weakening distance (D_c), and the yield stress (T_u). The fault is restricted to moving in a left-lateral direction; that is, the fault is not permitted to slip backward or vertically.

The synthetic parameters to be matched are strongly related to inversion solutions of data from the 2000 western Tottori earthquake (Peyrat and Olsen, 2004; Corish *et al.*, unpublished data, 2005). To maintain a strong resemblance to the real Tottori earthquake, the synthetic earth model also closely preserves the geometry and station distribution of the original fault (Figs. 1 and 2). The Tottori earthquake was chosen because of the wealth of high-resolution strong-motion data recorded near the fault and because of the relative simplicity of the rupture history suggested by kinematic inversion studies (Dalguer *et al.*, 2002; Iwata and Sekiguchi, 2002; Mikumo *et al.*, 2003).

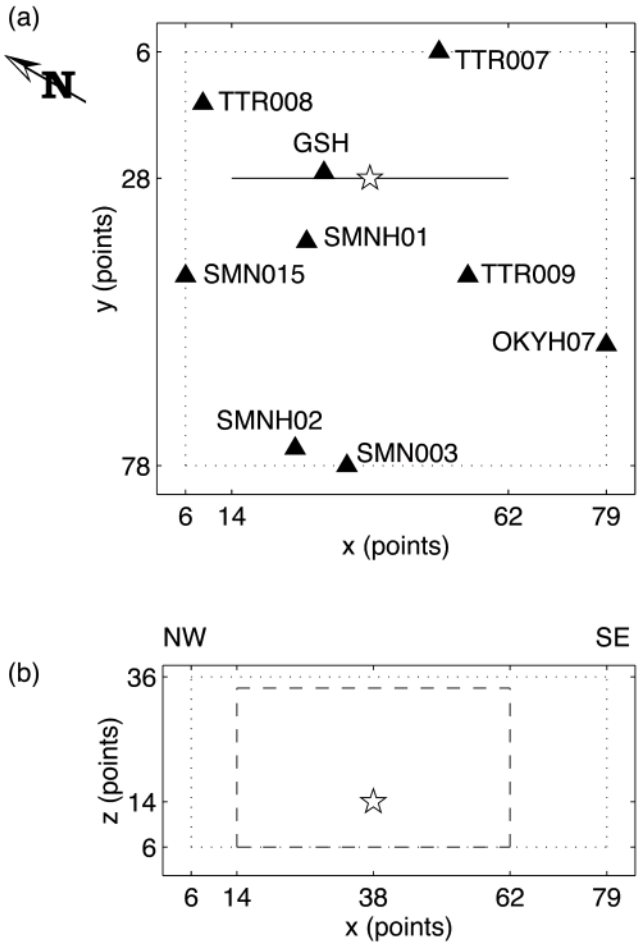

Figure 1. Earth model setup for the synthetic inversion. (a) Map view of the fault region, showing the fault trace and epicenter (star), and all strong-motion stations used for the inversion. Dimensions are given in grid coordinates; grid spacing is 500 m. (b) Cross section of the earth model as viewed from the southwest. The fault is outlined by dashed lines, and the hypocenter is marked with a star. The dotted lines in both diagrams show the extent of the boundary layers: a two-point free-surface boundary layer at the top of the model, and a five-point perfectly matched layers absorbing boundary condition along the remaining edges of the model.

Table 1
Velocity Structure Used for the Synthetic Earth Model*

V_p (km)	V_s (km)	ρ (g/cm^3)	Δ_z (km)
4.70	2.35	2.00	0.6
5.26	3.04	2.53	2.4
5.48	3.17	2.57	1.0
6.11	3.53	2.70	11.0
6.50	3.76	2.79	1.0

*V_p is the *P*-wave velocity, V_s is the *S*-wave velocity, ρ is the density, and Δ_z is the layer thickness. From the velocity structure for the Tottori, Japan region (Yagi, 2001).

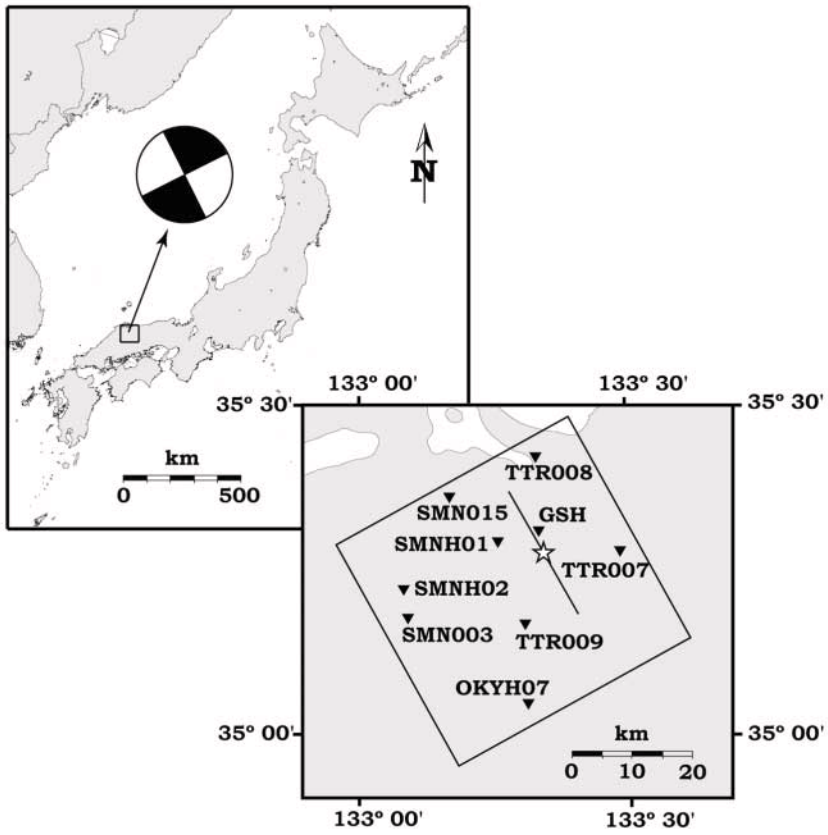

Figure 2. Map showing the location of the 2000 western Tottori earthquake, along with locations of nearby strong-motion stations (triangles) and the focal mechanism for the mainshock. The strong-motion stations are from the K-net and KiK-net networks operated by the National Institute for Earth Sciences and Disaster Prevention (Japan). The star marks the earthquake's epicenter.

The synthetic fault is composed of 18 rectangular cells, 4 by 5 km in size, each of which assumes a separate initial stress value between −2 and 5 MPa (Fig. 3). These fault patches are numbered from 1 through 18 in Figure 3 and will be referred to by number later in this article. In addition, a faultwide slip-weakening distance of 0.41 m and a uniform yield stress of 5 MPa are adopted. This parameterization allows a heterogeneous stress distribution on the fault but limits the number of parameters to a manageable number for the inversion. In the following discussion, the synthetic parameters used as the target for the inversion are called the "true parameters" or the "target parameters." The rupture history for the true parameters is shown in Figure 4. Rupture begins in a patch near the middle of the fault, and expands outward as the energy released during rupture pushes the stress level on the fault past the yield stress of the material. As the slip at a point on the fault increases, the stress at that point decreases to the dynamic sliding level, which is zero in this case. The rupture ends after about 7 sec.

The fault is parameterized in the same way for the inversion as for the target fault. The parameters sought include all 18 initial stress values, with allowed values between −2 and 5 MPa, and the slip-weakening distance, which has an allowed range of 0 to 1 m. The initial stress range was chosen by trial and error from inversions of real strong-motion data from the Tottori earthquake (Peyrat *et al.*, 2001; Peyrat and Olsen, 2004), and the domain for the slip-weakening distance is roughly based on the range of slip-weakening distances that have been found by several methods for Tottori and other earthquakes (e.g., Papageorgiou and Aki, 1983; Ide and Takeo, 1997; Mikumo *et al.*, 2003). For simplicity, the yield stress is held fixed in this inversion. Parameter selection is performed by using uniform random sampling within the regions defined by the nearest-neighbor cells. The parameters are permitted to vary independently from one another, and all parameters are weighted equally.

Least-squares misfit values are calculated between the known ground motion and the waveforms derived from each parameter set found by the neighborhood algorithm. A minimum of five grid points per wavelength is required to ensure accuracy of the fourth-order finite-difference scheme (Moczo *et al.*, 2000). From Table 1, the minimum *S*-wave velocity is 2350 m/sec, and if the smallest wavelength permitted is 2500 m, then the maximum resolvable frequency from the model is 0.94 Hz. Accordingly, the data are bandpass filtered between 0.05 Hz and 0.9 Hz using a fourth-order, single-pass Butterworth filter. The misfit between the filtered waveforms takes the form:

$$\text{misfit} = \sqrt{\sum_i \frac{(\text{true}_i - \text{predicted}_i)^2}{\text{true}_i^2}},$$

where the sums are taken over time. A uniform phase shift representing up to 3 sec for each seismic station is also permitted, and is subtracted before the misfit calculation is per-

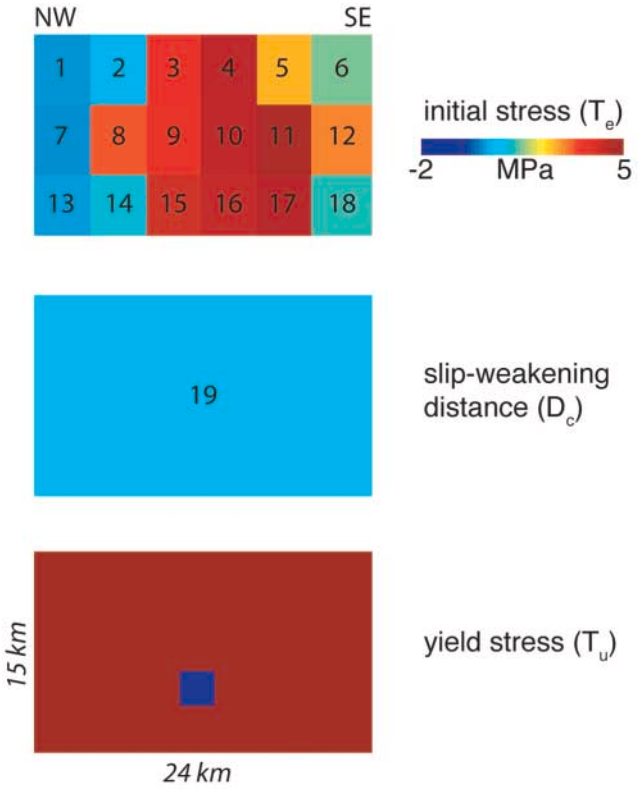

Figure 3. Cross-sectional views of the fault ($x - z$) plane showing the synthetic true parameters. Initial stress values range from -2 to 5 MPa (see Table 2 for a complete listing), and the slip-weakening distance is a uniform 0.41 m. The yield stress is 5 MPa across the fault, except in the 2.5-km-square rupture patch, where the yield stress is set to zero to induce rupture artificially. For the inversion, the yield stress is kept constant, but the initial stress values and slip-weakening distance are permitted to change. Numerals 1 to 19 are parameter indices that are referenced in the text and in other figures.

formed. Such a shift allows the inversion algorithm to recognize parameter values that are close to, but not exactly the true values as decent fits, since a main consequence of slightly perturbing parameter values is to introduce a phase shift in the waveforms. The shift asymptotically approaches zero as the misfit decreases.

Results

Preliminary results suggested that the neighborhood algorithm, like many other inversion schemes, is somewhat susceptible to local minima in the misfit surface. Although this effect is slight compared with the susceptibility of linear inversion methods, it is possible that results from a single inversion could be misleading. For this reason, a total of five 400-iteration inversions, identical except for the random seed used to initialize the search, were performed, and the results from all five inversions were combined. In all, more than 80,000 distinct combinations of parameters were considered. On 40 processors of the TeraGrid Itanium2 Linux cluster at the San Diego Supercomputing Center, each 400-iteration inversion took about 15 hr to complete. The finite-difference forward simulations took more than 99% of the computation time.

The minimum misfit per iteration is an indication of how efficiently the search algorithm finds good-fitting areas of the parameter space. This curve is plotted for each of the five inversions in Figure 5. In all five cases, the misfit decreases rapidly in the early stages of the inversion, but starts to level off as the iterations progress and never reaches a zero value. Performing additional iterations does not significantly improve the misfit. The neighborhood algorithm efficiently focuses the search into good-fitting regions of the parameter search during the first iterations, but its effectiveness drops as the search is narrowed. This drop in performance is a symptom of the strong nonlinearity of the dynamic rupture problem: if the correct solution is near a solution with a relatively high misfit, the exact solution might be assigned to a high-misfit nearest-neighbor cell, and passed over as the search progresses.

Because of the difficulty of arriving at a zero-misfit solution, it is important to collect information about the areas of the parameter space that generate low misfits to the known waveforms. A low misfit can be produced by a combination of several well-matched parameters and a few that are not well matched, and results with equally good-fitting seismograms often have different combinations of well- and poorly matched parameters. Thus, rather than relying exclusively on a single result for inferences about the state of the fault, it is preferable to perform a statistical analysis of a larger sample of results. Not only does such an analysis produce more robust estimates of the parameter values than examination of a single result, but it also delivers much more information about the relationship between the dynamic rupture parameters and the ground motion. For example, a statistical analysis reveals which parameters are well or poorly resolved by the inversion, which parameters contribute most strongly to the misfit, and what trade-offs between parameters might limit the amount of information that can be extracted from the data.

Table 2 and Figures 6 and 7 display some statistics of the 10% of parameter sets, or 8000 sets, with the lowest misfits to the true data. The 10% cutoff was chosen to illustrate the characteristics of the good-fitting areas of the parameter space, but different cutoff levels, say 5% or 20%, yield similar results. The mean parameter error, defined as $\text{err} = |\bar{x} - x_0|$, where $\bar{x}$ is the mean value of a parameter calculated from the top 10% of results, and x_0 is the true value of that parameter, is less than $\pm 14\%$ of the allowed range for each parameter for the 8000 best model sets. Figure 6 shows that the mean initial stress distribution of the best-fitting 10% of results captures the central stress asperity in the input parameters well, but that the error increases toward the edges of the main rupture area (compare with

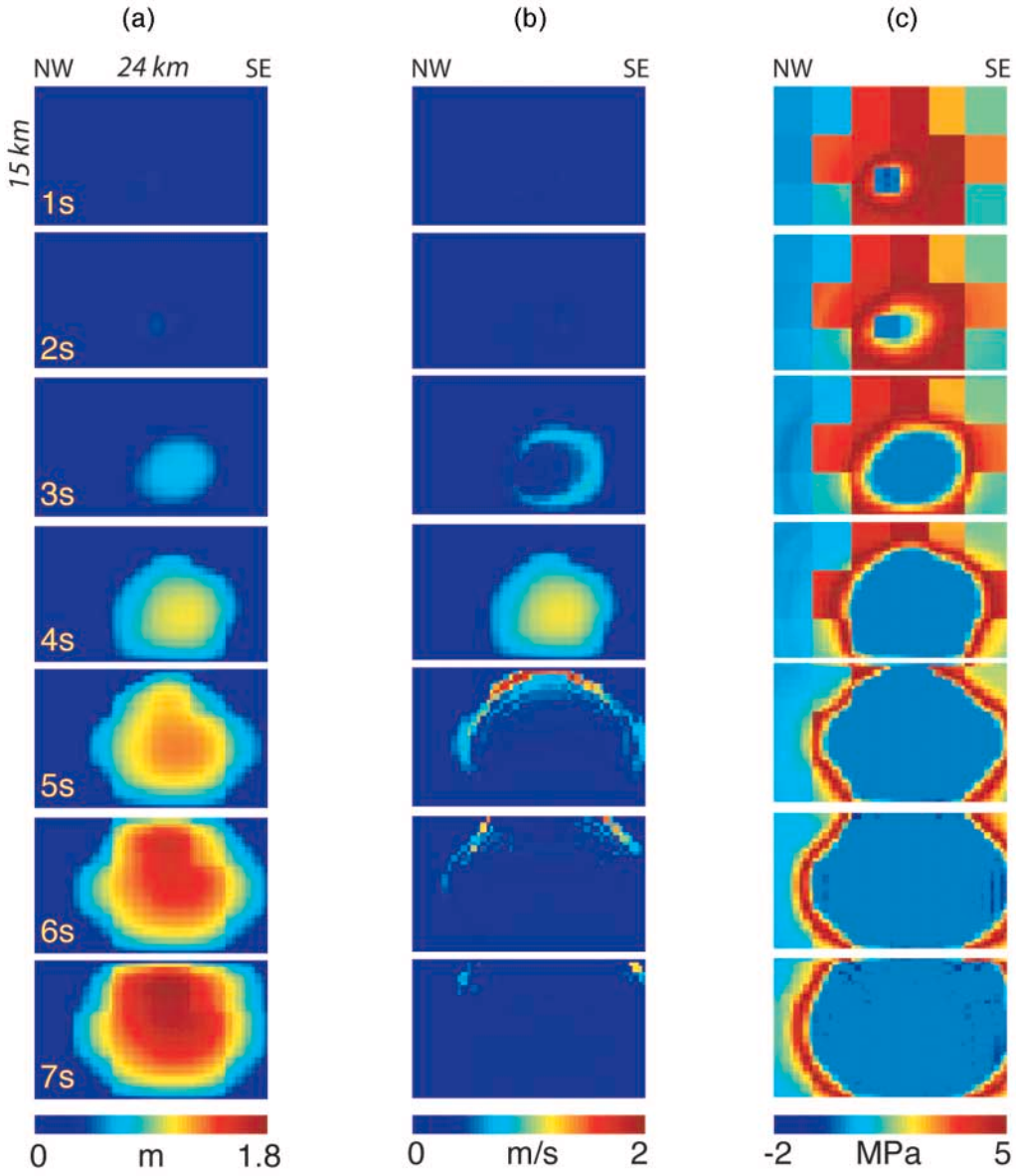

Figure 4. Rupture history for the true parameters. Each diagram is a snapshot of the vertical fault plane at a specific point in time. The time interval is 1 sec. Rupture is initiated artificially in a patch near the center of the fault, and spreads outward spontaneously as the rupture progresses. As the slip at a point on the fault increases to the slip-weakening distance (0.41 m), the stress decreases to zero. The rupture ends after about 7 sec. (a) Slip on the fault. (b) Slip rate. (c) Stress.

Fig. 4). The variance, computed as var $= 1/N\Sigma(x_i - \bar{x})^2$, displays a similar pattern: the variance is low in the central rupture area and increases toward outlying areas of the fault. Negative correlations occur between both the errors and the variances of the initial stress values with the total amount of slip in each region on the fault. This result is expected, as regions of the fault with high slip contribute more strongly to the ground motion than do regions with low slip, and therefore have a larger influence on the strong-motion records. Also, the parameter error and variance increase with depth, suggesting that the surface stations used for the inversion have trouble resolving the deeper parameters.

Figure 7 shows the distribution of parameter values in the 8000 best-fitting results. Most of the distributions are peaked around the true value of the parameter, confirming that, statistically, the inversion successfully locates the target values for most of the parameters. The parameters for which the distribution is not peaked near the true values are confined to the edges of the rupture area and the bottom of the fault. These parameters tend to have diffuse distributions,

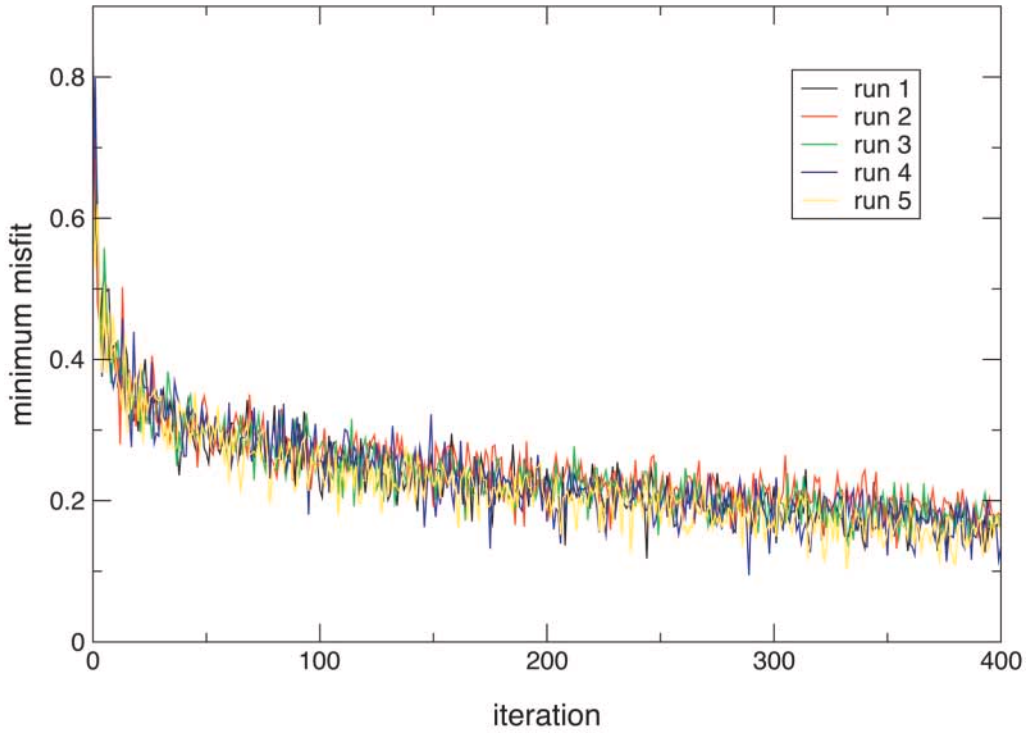

Figure 5. Minimum misfit per iteration for the five 400-iteration inversions.

Table 2

The 19 True Parameters Compared with the Parameter Values from the Best-Fitting 10% of the Inverted Models*

Parameter T_e	True Value (MPa)	Range (MPa)	Mean (MPa)	Median (MPa)	Error (MPa)	Normal Error (%)	Variance (MPa^2)
1	0.15	−2–5	−0.32	−0.36	−0.47	6.7	1.02
2	0.40	−2–5	0.42	0.44	0.02	0.3	0.84
3	3.77	−2–5	3.81	3.86	0.04	0.5	0.41
4	4.54	−2–5	4.24	4.34	−0.31	4.4	0.30
5	2.64	−2–5	2.91	2.90	0.26	3.8	0.81
6	1.45	−2–5	0.69	0.61	−0.75	10.8	1.83
7	0.11	−2–5	−0.61	−0.88	−0.71	10.2	1.19
8	3.33	−2–5	2.67	2.83	−0.66	9.5	1.73
9	3.80	−2–5	2.97	3.04	−0.83	11.8	0.60
10	4.51	−2–5	4.29	4.45	−0.22	3.2	0.33
11	4.89	−2–5	4.47	4.61	−0.42	6.0	0.23
12	3.02	−2–5	2.13	2.39	−0.89	12.7	2.61
13	0.20	−2–5	0.01	−0.19	−0.19	2.7	2.16
14	1.01	−2–5	1.94	2.26	0.93	13.2	3.76
15	4.23	−2–5	3.85	4.07	−0.38	5.4	0.87
16	4.42	−2–5	4.47	4.59	0.05	0.7	0.22
17	4.66	−2–5	3.91	4.13	−0.75	10.7	0.84
18	1.22	−2–5	2.17	2.45	0.94	13.5	4.06
D_c	True Value (m)	Range (m)	Mean (m)	Median (m)	Error (m)	Normal Error (%)	Variance (m^2)
19	0.41	0–1	0.32	0.33	−0.09	9.0	0.01

*Parameter indices correspond to the numbers in Figure 3. T_e is initial stress, and D_c is slip-weakening distance. The range comprises the values allowed by the inversion for each parameter. The mean, median, error, and variance are calculated for the best-fitting 10% of inverted models. Normalized error is computed as the error divided by the parameter range. The scalar error is $\mathrm{err} = \bar{x} - x_0$, and the variance is $\mathrm{var} = 1/N\Sigma(x_i - \bar{x})^2$. See also Figure 6.

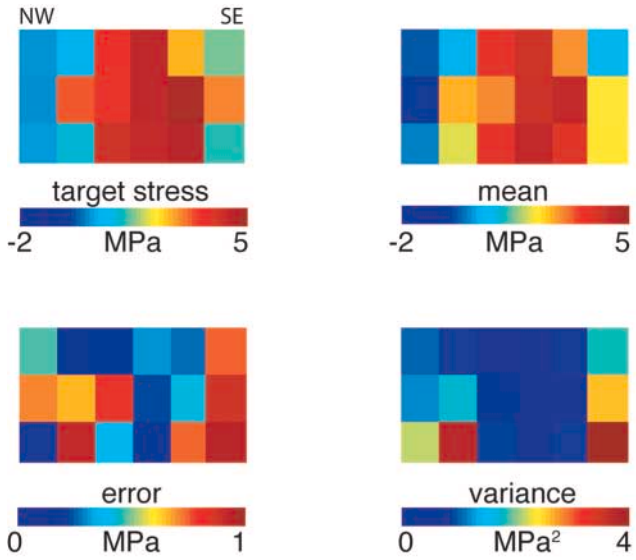

Figure 6. The target initial stress parameters compared with the mean parameter values of the best-fitting 10% of the 19-parameter inversion results. The mean parameter error, err $= |\bar{x} - x_0|$, and variance, var $= 1/N \sum (x_i - \bar{x})^2$, for the top 10% are also shown. These results, along with the analogous results for the slip-weakening distance parameter, are also detailed in Table 2.

suggesting that they are poorly constrained by the inversion. Parameters will be poorly constrained if they do not contribute strongly to the observed ground motion. That is, if changing a parameter's value has little effect on the waveforms observed at the surface stations, then the misfit should be relatively insensitive to that parameter.

An indication of the misfit's sensitivity to the individual parameters is shown in Figure 8. Starting from the best-fitting parameter set from the inversion, a single parameter is replaced in turn by a series of values spanning the entire parameter range. As one parameter is perturbed, all others retain their original values. After each change, a forward-rupture simulation is run and the misfit response is measured. If the misfit is very sensitive to a particular parameter, a strong change in the misfit value is expected as the parameter is perturbed. On the other hand, if the misfit is insensitive to a parameter, the misfit should remain flat as the parameter value is adjusted. In agreement with Figures 6 and 7, the misfit seems to be most sensitive to the parameters in the center of the fault, and especially to the parameters in the rupture nucleation area. Sensitivity drops off considerably at the sides and bottom of the fault. Nearly flat responses are observed for parts or all of the ranges for parameters 1, 7, 13, 14, and 18. Considering only the misfit values, the set of parameters containing a value of -2 MPa for parameter 13 is nearly indistinguishable from the set containing a value of 3.5 MPa for the same parameter. Thus, for low-sensitivity parameters, there is not enough information in the waveforms for the inversion to identify the exact solution. A limitation of our computational scheme is illustrated here. We are band limited in the forward modeling and limited to a realistic representation of the station distribution. As a result, the nonideal station distribution cannot resolve portions of the rupture plane and the frequency limits on the seismograms limit our ability to capture the precise rupture timing.

Correlations among parameters are not included in the misfit sensitivity analysis. The misfit might respond differently to a change in a combination of parameters than it does to changes in single parameters. For example, performing the misfit-sensitivity test starting from a different starting set: the mean of the top 10% of results, rather than the best-fitting result, gives misfit-response curves similarly shaped to the ones shown in Figure 8, but the preferred slip-weakening distance changes by 20 cm, from 0.55 m to 0.35 m. In fact, the slip-weakening distance is correlated with the initial stress parameters because both parameters influence the slip at a particular point on the fault, and a change in the mean initial stress value favors a different slip-weakening distance. Figure 9 plots the slip-weakening distance from the top 10% of parameter sets versus the faultwide mean initial stress. A positive, linear correlation exists between the two: the linear correlation coefficient is $R = 0.61$, and a linear regression for the data gives the relationship $D_c = 0.31\bar{T}_e - 0.44$, where D_c is in meters and $\bar{T}_e$ is in megapascal. Previous work has shown that intrinsic trade-off exists between the yield stress and the slip-weakening distance (Guatteri and Spudich, 2000) and between the yield stress and the initial stress (Peyrat *et al.*, 2001, 2004). The results of the current study confirm that a trade-off between the slip-weakening distance and the mean initial stress also exists.

It has been suggested that dynamic rupture simulations should be performed with grid spacings small enough to capture changes in the slip rate and rupture velocity within the slip-weakening zone at the tip of the fault. The slip-weakening zone is defined as the part of the fault behind the rupture front where the stress is decreasing from the static yield stress to the dynamic frictional sliding level. For the stress-glut formulation, roughly 10 grid points should span the slip-weakening zone (Dalguer and Day, 2006). For a crack advancing with negligible velocity, the size of the slip-weakening zone is given by (Day *et al.*, 2005):

$$\Lambda = \frac{9\pi}{32} \frac{\mu^* D_c}{T_u - T_f},$$

where μ^* is the effective elastic modulus of the material appropriate for a mode II or mode III crack, and T_f is the dynamic frictional sliding stress, which, in this study, is 0. Under conditions of negligible velocity, the synthetic fault modeled here has a slip-weakening zone of about 800 m, suggesting that a grid spacing of about 80 or 100 m is desirable. Because of the time required to perform each forward simulation, the grid spacing used in this investigation, 500 m, is at least five times larger than the 80- to 100-m guidepost.

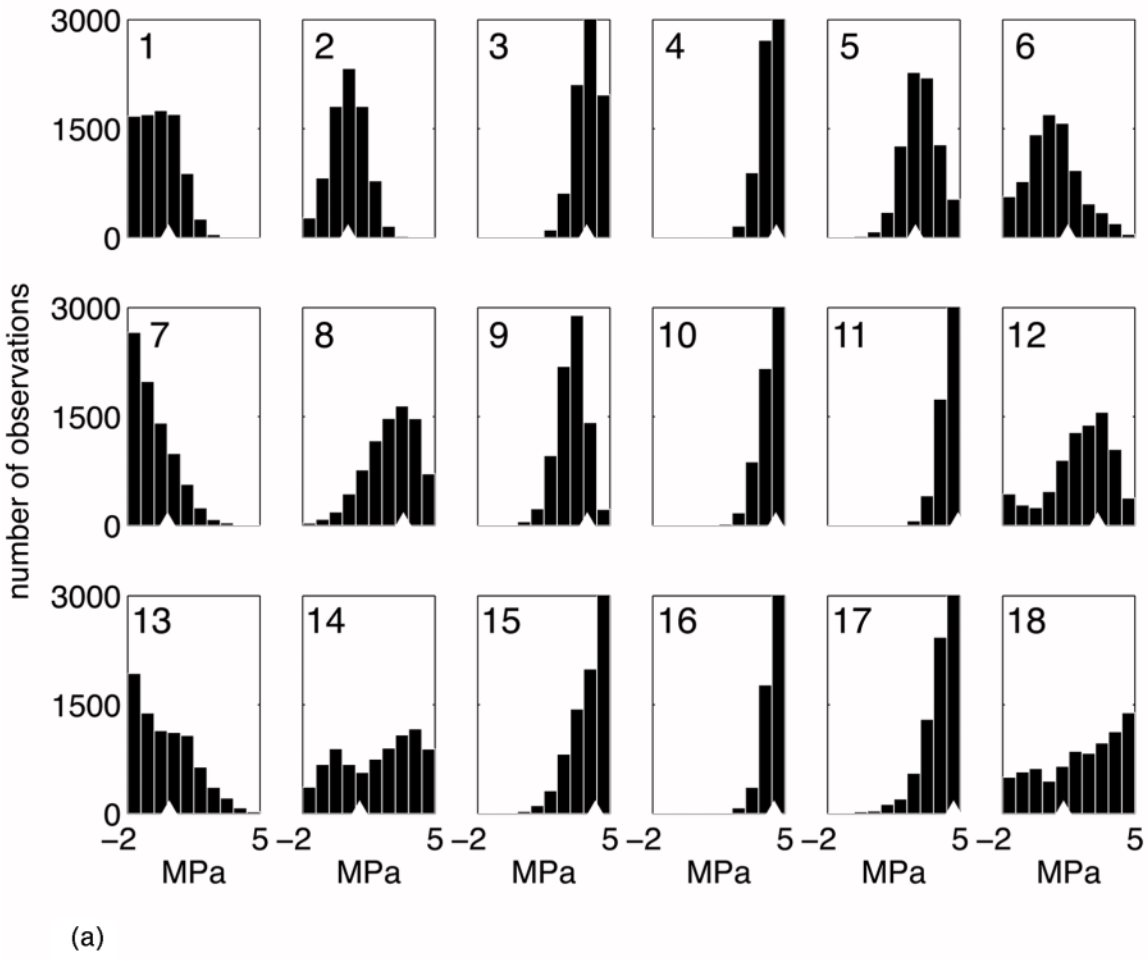

Figure 7. (a) Histograms of the best-fitting 10% of inversion results, showing the distribution of values found by the inversion for each initial stress parameter. The total number of parameter sets in the top 10% is 8000. Note that the initial stress cannot exceed 5 MPa, which is the yield stress value. The white caret indicates the true parameter value. The numbers inside each diagram refer to the parameter locations shown in Figure 3. (b) Histogram of the slip-weakening distance values from the best-fitting 10% of inversion results. The white caret shows the true slip-weakening distance.

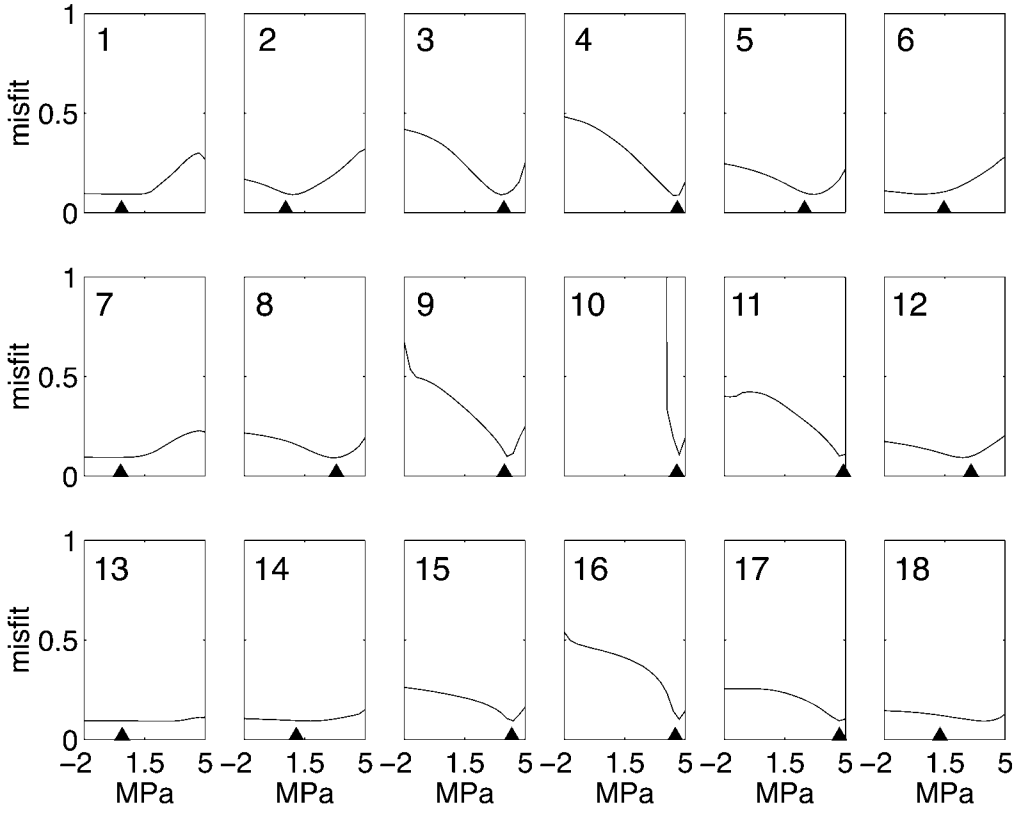

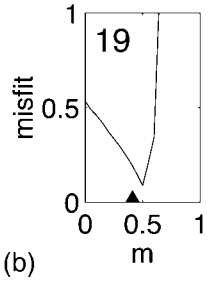

Figure 8. (a) Sensitivity of the misfit to perturbations in individual initial stress parameters. Starting from the parameter values from the best-fitting inverted result, a single parameter is replaced in turn by a series of values spanning the entire parameter range. All other parameters remain unchanged. Forward simulations are recalculated, and the resulting misfits are plotted. Solid lines show the misfit curve, and the carets give the true value of the parameter. The numbers in each diagram refer to the parameter locations shown in Figure 3. (b) The same experiment repeated for the slip-weakening distance. The solid line is the misfit curve, and the caret is the true slip-weakening distance.

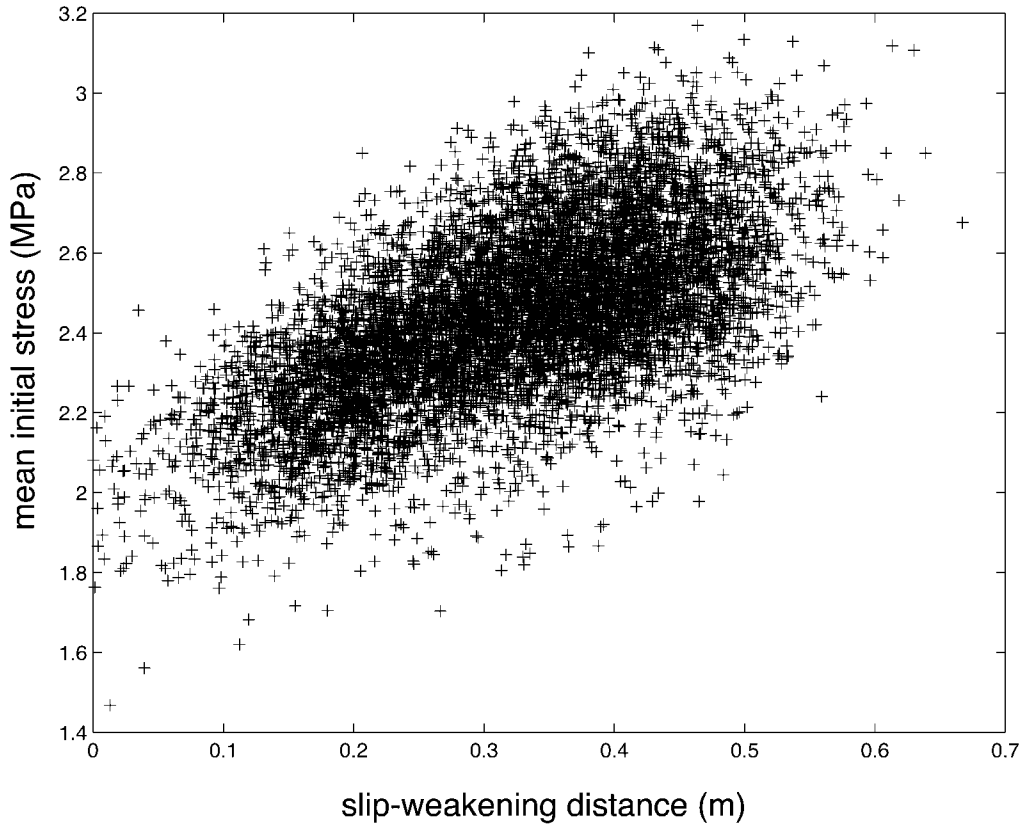

Figure 9. The top 10% of results plotted as a combination of the faultwide mean initial stress and the slip-weakening distance. There is a positive, linear correlation between the mean initial stress and the slip-weakening distances found by the inversion: for the best-fitting 10% of results, a linear regression gives $D_c = 0.31\,\bar{T}_e - 0.44$, and $R = 0.61$.

To quantify the differences introduced by running the forward simulation at 500 m instead of 100 m, the model is adapted to a 100-m grid and the forward problem for the true parameters is rerun. The seismograms associated with the 100-m true model and those of the 500-m true model are compared in Figure 10. Both sets of seismograms are bandpass filtered between 0.05 Hz and 0.9 Hz. The misfit between these seismograms is 0.210, a value that would place the 100-m solution among the top 5% of the results for the 500-m inversion. Most of the misfit is in the form of a time delay of about 0.35 sec for the 500-m waveforms relative to the 100-m arrivals. In order to compensate for the slower rupture propagation time for larger grid sizes, a 500-m grid would likely underestimate the slip-weakening distance, or slightly overestimate the initial stress values present in the real earth. Either of these alterations would effectively speed up the rupture evolution.

Discussion and Conclusions

The dynamic rupture parameters on a fault, including the initial stress and slip-weakening distance, are important keys to predicting where and when the fault will fail, but they are difficult to estimate from field observations. Seismologists are often left to infer these parameters from the results of numerical inversions of large earthquakes. As dynamic inversions become more widely used to match real data, the need to recognize the specific capabilities and limitations of these methods takes on a greater importance. To date, much more work has been done to develop methods of dynamic rupture inversion than to assess how well these methods work. The investigation presented here has addressed the latter problem.

Nonlinear inversion problems are challenging because the relationship between the misfit and the parameters is often complicated and unpredictable, and simultaneously inverting for many parameters compounds these difficulties. Because of the strong nonlinearity of the dynamic rupture problem, and the impossibility of conducting an exhaustive search of the parameter space, the chances of finding an exact solution for the parameter values are very slim. However, using a parameter search method such as the neighborhood algorithm, it is possible to localize the parameter estimates to reduced areas of the parameter space near the true values. The results of this study have shown that both the initial stress and the slip-weakening distance values can

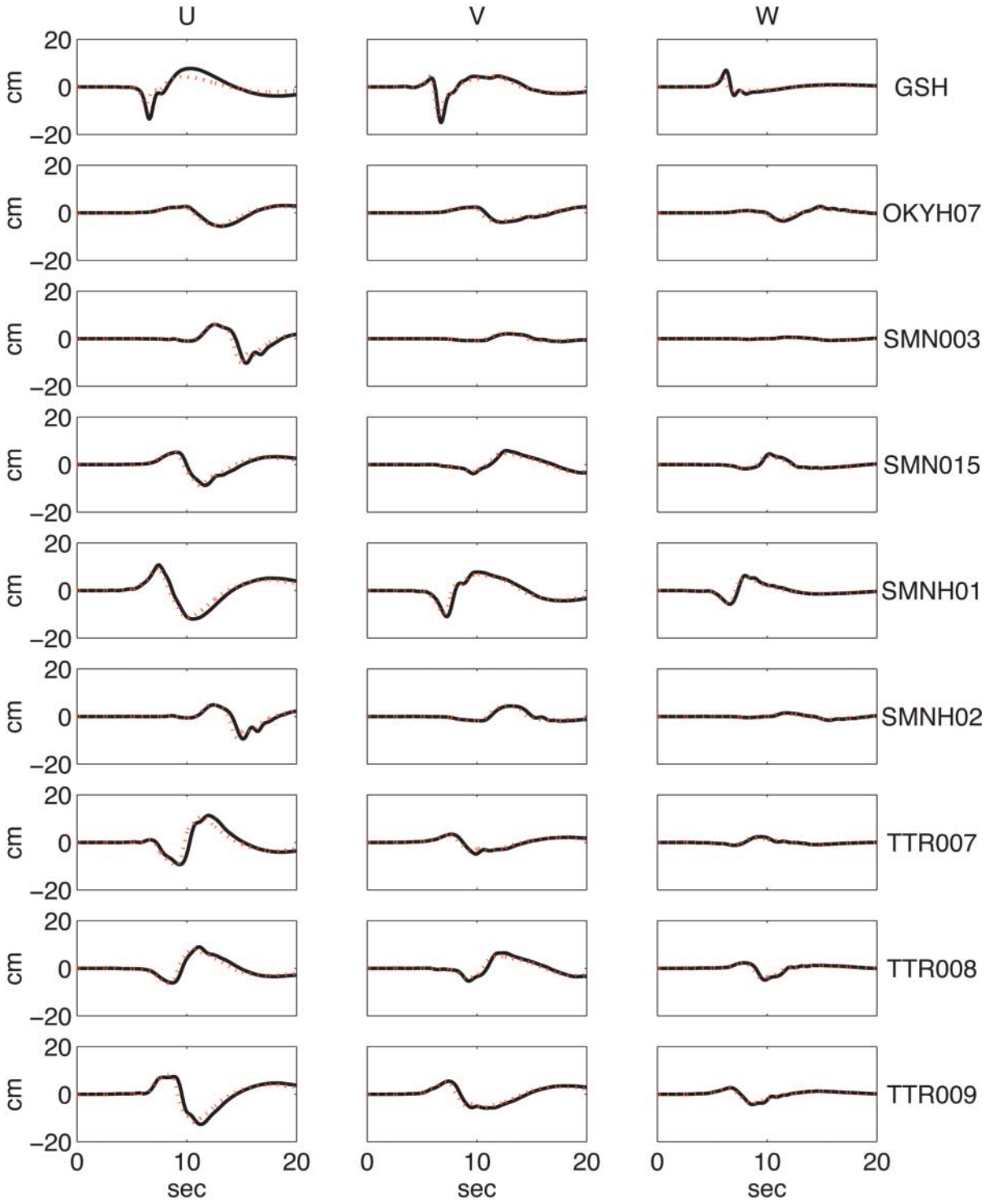

Figure 10. True model ground displacement calculated for different grid spacings. *U* is the fault-parallel direction, *V* is fault-perpendicular, and *W* is vertical. The solid black trace shows the ground motion for the true parameters calculated at a grid spacing of 500 m, and the dotted red line shows the ground motion for the same parameters calculated at 100-m grid spacing. The misfit between the two sets of strong-motion records is 0.210.

be estimated, within a reasonable amount of error, from a statistical analysis of the low-misfit inversion results. Averaging many good-fitting results from several independent inversions yields robust estimates of the true parameter values, and examining the distributions of the parameters in the sample gives a good idea of how well each parameter is resolved. The results of rupture inversions frequently are reported as a single set of parameter values or a small collection of these sets that represent the best fit to the seismic data, but this study indicates that a statistical evaluation of a larger set of results is much more powerful.

Assessment of the inversion results also reveals that different combinations of parameters can have misfits similar to the observed ground motion. For instance, there is a trade-off between the mean initial stress on the fault and the slip-weakening distance that precludes identification of the exact values of either quantity based on strong-motion records. This trade-off occurs because both the initial stress and the slip-weakening distance affect the amount and timing of slip on the fault. For instance, slip at a point on the fault increases with the stress drop ($T_e - T_f$) and decreases with increasing slip-weakening distance. Various combinations of the initial stress and the slip-weakening distance can result in very similar slip response, and the ground-motion data are unable to identify the exact combination present in the target parameters. This limitation must be acknowledged when reporting dynamic inversion results.

Uncertainties in the earth model are not addressed by the current study because the inversion setup is an exact replica of the true model. For inversions of real data rather than synthetic data, however, there are many more, and often unknown sources of error caused by approximating the earth by an idealized model. Potential sources of error include oversimplification of the parameters, inaccuracies in the velocity structure, misrepresentation of the fault geometry on a rigid grid, station distribution, specific site effects for each station, and failure to model accurately any inelastic behavior of the materials. Despite these complications, however, many of the methods used in this study have direct applications to inversions from real data. For instance, although an error measure like the one shown in Figure 8 cannot be calculated when the true parameters are unknown, it is possible to calculate the variance in a subset of the inverted parameters. Although the correlation between variance and error is not exact, the variance in the inversion results does give some idea as to the ability of the inversion to determine reliable parameter values. If the variance for a parameter is high, then the parameter is probably poorly constrained by the inversion. If it is low, however, caution is still warranted in interpreting the results. A low variance could be due to a persistent local minimum or trade-off between parameters. Misfit response curves like the ones in Figure 10 can also be constructed from real-data inversion results. Such plots can further help to separate well-constrained parameters from those that are poorly constrained, and can also be used to mark out the shape of the good-fitting portions of the parameter space. However, these plots too must be treated with caution because correlation between the parameters might strongly affect the shape of the misfit-response curve.

Dynamic rupture inversion is a useful tool for understanding how fault-plane conditions combine to cause earthquake ruptures. However, before any interpretations about the system modeled can be made with confidence, it is imperative to recognize what limitations in the data, the model, or the inversion method might preclude identification of the actual parameters. Typically, the best-fitting parameter sets discovered by an inversion command the most attention, but in fact, a comprehensive examination of a larger set of results is much more informative. Details of the parameter space resolution, potential trade-offs between parameters, and certain pitfalls in the inversion process can be identified only by examining the variations among a large group of results. Including a systematic assessment of the inverted solutions as a regular part of the inversion process will help to extract more information about the dynamic rupture parameters from the inversion, and will also help to identify where more research is needed to further understand fault rupture.

Acknowledgments

We thank Sophie Peyrat for access to many of her results and for her help with the inversion code, and Jim Gattiker for discussions about the statistical aspects of this study. We are grateful to Pengcheng Liu, Daniel Lavallee, and Anders Niklasson for their ideas and comments. We would also like to thank two anonymous reviewers for their insightful comments. Much of the work done for this project was performed at Los Alamos National Laboratory under a University of California and Los Alamos National Laboratory cooperative research agreement, UC-LANL CARE grant UR5P. The project was partly supported by NSF award EAR0424065 (K.B.O.). In addition, S. Corish was supported in part by a UC Regents Fellowship. This document has been approved for public release by Los Alamos National Laboratory as an unclassified report, LA-UR-06-2316.

References

Andrews, D. J. (1976). Rupture propagation with finite stress in antiplane strain, *J. Geophys. Res.* **81,** 3575–3582.

Andrews, D. J. (1999). Test of two methods for faulting in finite-difference calculations, *Bull. Seism. Soc. Am.* **89,** 931–937.

Cotton, F., and M. Campillo (1995). Frequency domain inversion of strong motions; application to the 1992 Landers earthquake, *J. Geophys. Res.* **100,** 3961–3975.

Dalguer, L. A., and S. M. Day (2006). Comparison of fault representation methods in finite difference simulations of dynamic rupture, *Bull. Seism. Soc. Am.* **96,** 1764–1778.

Dalguer, L., K. Irikura, W. Zhang, and J. D. Riera (2002). Distribution of dynamic and static stress changes during 2000 Tottori (Japan) earthquake: brief interpretation of the earthquake sequences; foreshocks, mainshock and aftershocks, *Geophys. Res. Lett.* **29,** no. 16, 1758.

Day, S. M. (1982). Three-dimensional simulation of spontaneous rupture: the effect of nonuniform prestress, *Bull. Seism. Soc. Am.* **72,** 1881–1902.

Day, S. M., L. Dalguer, N. Lapusta, and Y. Liu (2005). Comparison of finite difference and boundary integral solutions to three-dimensional spontaneous rupture, *J. Geophys. Res.* **110,** B12307.

Gottschaemmer, E., and K. B. Olsen (2001). Accuracy of the explicit planar free-surface boundary condition implemented in a fourth-order

staggered-grid velocity-stress finite-difference scheme, *Bull. Seism. Soc. Am.* **91,** 617–623.

Graves, R. W. (1996). Simulating seismic wave propagation in 3D elastic media using staggered-grid finite differences, *Bull. Seism. Soc. Am.* **86,** 1091–1106.

Guatteri, M., and P. Spudich (2000). What can strong-motion data tell us about slip-weakening fault-friction laws? *Bull. Seism. Soc. Am.* **90,** 98–116.

Ida, Y. (1972). Cohesive force across the tip of a longitudinal-shear crack and Griffith's specific surface energy, *J. Geophys. Res.* **77,** 3796–3805.

Ide, S., and M. Takeo (1997). Determination of constitutive relations of fault slip based on seismic wave analysis, *J. Geophys. Res.* **102,** 27,379–27,391.

Iwata, T., and H. Sekiguchi (2002). Source prestress and near-source ground motion during the 2000 Tottori-ken Seibu earthquake, *Proceedings of the 11th Japan Earthquake Engineering Symposium* (in Japanese with English abstract).

Madariaga, R., K. B. Olsen, and R. Archuleta (1998). Modeling dynamic rupture in a 3D earthquake fault model, *Bull. Seism. Soc. Am.* **88,** 1182–1197.

Marcincovich, C., and K. B. Olsen (2003). On the implementation of perfectly matched layers in a three-dimensional fourth-order velocity-stress finite difference scheme, *J. Geophys. Res.* **108,** 2276.

Mikumo, T., K. B. Olsen, E. Fukuyama, and Y. Yagi (2003). Stress-breakdown time and slip-weakening distance inferred from slip-velocity functions on earthquake faults, *Bull. Seism. Soc. Am.* **93,** 264–282.

Moczo, P., J. Kristek, and L. Halada (2000). 3D fourth-order staggered-grid finite-difference schemes; stability and grid dispersion, *Bull. Seism. Soc. Am.* **90,** 587–603.

Olsen, K. B. (1994). Simulation of three-dimensional wave propagation in the Salt Lake Basin, *Ph.D. Thesis,* University of Utah, Salt Lake City.

Papageorgiou, A. S., and K. Aki (1983). A specific barrier model for the quantitative descroption of inhomogeneous faulting and the prediction of strong-ground motion, part II: Applications of the model, *Bull. Seism. Soc. Am.* **73,** 953–978.

Peyrat, S., and K. B. Olsen (2004). Nonlinear dynamic rupture inversion of the 2000 western Tottori, Japan, earthquake, *Geophys. Res. Lett.* **31,** 1–4.

Peyrat, S., K. B. Olsen, and R. Madariaga (2001). Dynamic modeling of the 1992 Landers earthquake, *J. Geophys. Res.* **106,** 26,467–26,482.

Peyrat, S., K. B. Olsen, and R. Madariaga (2004). Which dynamic rupture parameters can be estimated from strong ground motion and geodetic data? *Pure Appl. Geophys.* **161,** 2155–2169.

Sambridge, M. (1999). Geophysical inversion with a neighbourhood algorithm. I. Searching a parameter space, *Geophys. J. Int.* **138,** 479–494.

Yagi, Y. (2001). Source rupture process of the Tottori-ken Seibu earthquake of Oct. 6, 2000, obtained by joint inversion of near-field and teleseismic data, Presented at the Meeting of Japan Earth and Planetary Sciences, Tokyo, Japan, May 2001.

Zhang, W., T. Iwata, K. Irikura, H. Sekiguchi, and M. Bouchon (2003). Heterogeneous distribution of the dynamic source parameters of the 1999 Chi-chi, Taiwan, earthquake, *J. Geophys. Res.* **108,** 2232.

Geophysics Group
Los Alamos National Laboratory
Los Alamos, New Mexico 87545
corish@lanl.gov
cbradley@lanl.gov
(S.C., C.B.)

Department of Geological Sciences
San Diego State University
San Diego, California 92182
kbolsen@sciences.sdsu.edu
(K.O.)

Manuscript received 25 March 2006.